**Nanocomposites of Nickel Oxide and Zirconia for the Preparation of Photocathodes with Improved Performance in p-Type Dye-Sensitized Solar Cells**

# Nanocomposites of nickel oxide and zirconia for the preparation of photocathodes with improved performance in *p*-type dye-sensitized solar cells

Matteo Bonomo[a*], Paolo Mariani [b], Francesco Mura[a], Aldo Di Carlo [b,c] and Danilo Dini[a*]

*(a) Department of Chemistry, University of Rome LA SAPIENZA, P.le A. Moro 5, 00185 Rome, Italy*
*(b) Dept. of Electronic Engineering, University of Rome "Tor Vergata", via del Politecnico 00133 Rome, Italy.*
*(c) National University of Science and Technology "MISiS", 4, Leninsky Prosp., Moscow 119049, Russian Federation*



## ABSTRACT

In *p*-type dye sensitized solar cells (*p*-DSCs) with nickel oxide (NiO) based photocathodes one of the main causes of their relatively poor photoconversion performances is the fast recombination between the photoinjected holes in the valence band of the *p*-type semiconductor and the reduced form of the redox shuttle (typically $I^-$). As a matter of fact, recombination phenomena at the NiO/electrolyte interface heavily limit both photovoltage and photocurrent. Different approaches have been adopted to minimize such an unwanted process: these range from the pretreatment of the electrode surface with NaOH to the employment of passivating organic molecules (e.g. CDCA) in the sensitizing solution and/or in the electrolyte solution. The present contribution describes the implementation of the addition of zirconia ($ZrO_2$) nanoparticles in nanostructured NiO films as anti-recombination agent in *p*-DSCs due to the electro-inactivity of $ZrO_2$. $ZrO_2$ nanoparticles with diameter, Ø, of 20 nm, and NiO nanoparticles with Ø < 50 nm were dispersed together in the paste precursor for screen-printing. Different compositions of the mixture of NiO and $ZrO_2$ nanoparticles were considered. From the combined analysis of the electrochemical and photoelectrochemical properties of different nanocomposites it was concluded that the molar ratio $ZrO_2$/NiO had the optimal range of 2-5 % for realizing photocathodes more efficacious than sole nanostructured NiO. Among the nanocomposite photoelectrodes the one obtained from the inclusion of 2% of $ZrO_2$ nanoparticles produced the better photoelectrochemical performance being the short-circuit current density $J_{SC}$ = 2.037 mA/cm$^2$ and the overall efficiency $\eta$ = 0.088% when P1 is the sensitizer. These results show an increase up to 40% compared to the un-modified NiO electrode. The unexpectedly low efficiency of electrode with molar ratio of zirconia in nickel oxide of 5% was associated to an insufficient dye-loading on NiO, in combination to the increase of the percentage of the photoelectrochemically inert $ZrO_2$ additive. The electrochemical impedance spectroscopy (EIS) data of the complete device under illumination confirmed that the improvement is mainly due to an increase of the recombination resistance, $R_{rec}$, ongoing from sole nanostructured NiO ($R_{rec}$ = 56.3 Ω) to the electrode obtained from the nanocomposite with molar ratio $ZrO_2$/NiO = 0.02 ($R_{rec}$ = 70.3 Ω).

* corresponding author, email: matteo.bonomo@uniroma1.it danilo.dini@uniroma1.it

## INTRODUCTION

Among photovoltaic technologies the monocrystalline silicon-based devices and lead iodide based perovskite solar cells are capable to reach conversion efficiencies up to 20% under solar irradiation[1]. When indoor illumination with diffuse features is considered as source of luminous energy the dye-sensitized solar cell (DSC)[2] appears as the most effective choice despite the fact that the highest efficiency of a DSC is below 15%[3]. More recently, Gräetzel[4] and co-workers reported overall efficiency up to 30% when the source intensity is as low as 100 lux. Conversions up to 40% could be theoretically achieved by creating a p-n junction[5] (i.e. by coupling a photoanode to a photocathode) when the solar radiation is considered as excitation source. Such a tandem configuration would sensibly reduce also the costs of production of the corresponding device. The theoretical limit of 40% is still far to be reached because of the generally poor performance of photocathodes. To our knowledge, the best performance reported so far for a *p*-type DSC (*p*-DSC) is lower than 2% under 1 Sun of illumination[6]. One of the main causes of this is the fast recombination reaction that occurs between the photoinjected holes in the valence band (VB) of the photocathode (usually made of NiO)[7–10] and the reduced form of the redox shuttle (typically the iodide anion)[11–13]. In fact, recombination phenomena at the NiO/electrolyte interface heavily limit both photovoltage and photocurrent. The photoinjected holes are mainly localized onto NiO surface in correspondence of the electron-deficient $Ni^{3+}$ sites. Different approaches have been adopted to minimize such an unwanted reaction. The rational design of a sensitizer with bulky substituents[6,14,15] could help to keep iodide distant from the holes localized on the electrode surface. The implementation of a NiO compact layer has been proved to reduce recombination phenomena at the electrolyte/FTO interface[16–18]. Metal-doping or UV irradiation of NiO electrode are feasible approaches to tune the opto-electronic properties of photocathode but are as not effective in reducing the interfacial recombination[19–21]. An alternative route is the direct modification of the photocathode. In a previous paper we showed that the treatment of NiO surface with soda has a twofold effect: it reduces the surface concentration of superficial $Ni^{3+}$ sites and passivates the NiO surface prior sensitization[22]. The success of this method has been confirmed by the achievement of a less dark film. Unfortunately, the reduction of the number of $Ni^{3+}$ sites lowered also the amount of loaded sensitizer leading to a less performing device (lower photocurrent). We also tested CDCA (chenodeoxycholic acid) in squaraines-based p-DSC[23]. In that work CDCA (acting as both disaggregating and passivating agent) was added in the sensitizer solution with a concentration of 20 mmol. The overall efficiency was enhanced by 25% due to the depression of dye aggregation. Nevertheless, the amount of chemisorbed dye was lowered because of the competition between sensitizer and CDCA in binding $Ni^{3+}$ sites. To avoid the latter phenomena, Odobel *et al.*[24] dissolved CDCA (50 mM) in the electrolyte. They reported an enhancement of the 20 % of the conversion efficiency due mainly to a higher $V_{OC}$ whereas the $J_{SC}$ was substantially unchanged. The employment of an insulating layer of $Al_2O_3$ was proposed by Uehara and coworkers[25] but it diminished the electron injection of surface chemisorbed sensitizer more than the desired recombination phenomena Natu and co-authors reported the implementation of a more efficient $Al_2O_3$ insulating layer directly deposited onto the NiO electrode by Atomic Layer Deposition[26]. Yet, the enhancement of photoelectrochemical properties is modest. As far as we are aware, no research group previously attempted the nanometric approach in the framework of DSCs with the preparation of the nanocomposites here reported. In particular, throughout this work we described, for the first time, the employment of $ZrO_2$ nanoparticles, NPs, with diameter Ø < 20 nm) as not electroactive additive in NiO electrodes for *p*-DSC application. $ZrO_2$ is an insulating oxide with a bandgap higher than 5 eV. We expect that the presence of zirconia nanoparticles, i.e. a nanostructured version of $ZrO_2$ with strong tendency of being finely dispersed on the electrode surface, diminishes the portion of NiO exposed to the electrolyte thus diminishing the probability with which $Ni^{3+}$ sites on the surface recombine with the redox shuttle. The effect of NiO dilution imparted by of zirconia nanoparticles on the electrode surface brings necessarily about the

consequent minimization of recombination phenomena at the electrode/electrolyte interface as well as flux of photoinjected charges in the photocathode. The purpose of this study is to evaluate to which extent the presence of $ZrO_2$ NPs favors the suppression of recombination without being excessively detrimental against dye-loading and photoinjection on the NiO portions of the nanocomposite. $ZrO_2$ has been chosen because of its chemical inertness and long-term stability. The formation of a mixed oxide of nickel and zirconium with a structure distinct from the ones of NiO and $ZrO_2$ has not been evidenced (vide infra)[27]. Therefore, the attainment of a solid solution from the mixing and the sintering of NiO and $ZrO_2$ NPs is reasonably excluded. On these bases we expect that the nanocomposites are actually constituted by two segregated oxides.

## EXPERIMENTAL PART

The chemicals ethylcellulose, α-terpineol, NiO nanopowders, ethanol and acetonitrile (ACN) were purchased from Fluka or Sigma-Aldrich whereas $ZrO_2$ nanoparticles were purchased from US Research Nanomaterials. All chemicals were used without any further treatment of purification.
The experimental procedure to produce NiO/$ZrO_2$ slurry consists on a modified version of the one reported in our previous paper[28,29]: an ethanol solution of NiO nanopowders (6 g), $ZrO_2$ nanospheres (variable amount), α-terpineol as solvent (20 g) and ethylcellulose as crosslinker were mixed together under continuous stirring. Then this solution was slowly heated at 50 °C to let completely evaporate the solvent. The resulting slurries were screen-printed over 2.2 mm thick FTO/glass substrates (TEC7 from NSG), which were previously cleaned in an ultrasonic bath with acetone for 10 min and successively with isopropyl alcohol for 10 min. The electrodes with geometrical area of 0.36 $cm^2$, were annealed at 450 °C in oven for 30 minutes. The thickness of the annealed samples ranged between 2 and 3 μm (evaluated with a Dektak 150® profilometer from Veeco). The morphology has been investigated with a FESEM Auriga Zeiss Field Emission. EDX (EDX Quantax Bruker, Resolution 123 eV (Mn $K_\alpha$) was employed for the elemental analyses. The amount of added $ZrO_2$ varied from 0 (pure NiO) to 856 mg (corresponding to the molar ratio $ZrO_2$/NiO = 0.11). Six slurries have been prepared with different values of $ZrO_2$/NiO molar ratio:

- Pure NiO as reference
- $ZrO_2$/ NiO = 0.001, with 8 mg of $ZrO_2$
- $ZrO_2$/ NiO = 0.010, with 85.6 mg of $ZrO_2$
- $ZrO_2$/ NiO = 0.020, with 171.2 mg of $ZrO_2$
- $ZrO_2$/ NiO = 0.053, with 428 mg of $ZrO_2$
- $ZrO_2$/ NiO = 0.111, with 856 mg of $ZrO_2$

The resulting slurries were chemically and physically stable for several months in ambient conditions. Throughout the paper, each electrode made starting from these slurries has been named as NiO_$ZrO_2$_X where X represents the $ZrO_2$/NiO molar ratio.

The electrochemical characterization of $ZrO_2$/NiO samples consisted in the recording of cyclic voltammetries (CVs), and electrochemical impedance spectra with Autolab potentiostat/galvanostat Mod. PGSTAT12® from Metrohm. PGSTAT was remotely controlled from a computer by means of the software Nova 1.9. The electrochemical cell had a three-electrode configuration with NiO (either bare or $ZrO_2$-modified as nanocomposite) as working electrode, a platinum wire as the counter-electrode and Ag/AgCl electrode as the reference electrode. The supporting electrolyte was 0.1 M $LiClO_4$ in ACN. With regard to the CV measurements the applied potential has been varied from -0.27 to 1.13 V with a variable scan rate (10, 20, 50, 100 or 200 $mV*s^{-1}$). Impedance spectra were recorded in the same experimental set up by applying a frequency value ranging from 100 KHz to 0.1 Hz with a potential amplitude of stimulus of 20 mV.

WAXS experiments were carried out on a Bruker D8 Advance with DaVinci design diffractometer (angle dispersive). The diffractometer is equipped with a Cu Kα X-Ray tube (λ = 1.5406 Å). The instrument is fitted with focusing Göbel mirrors along the incident beam and Soller slits on both incident and diffracted (radial) beams. Data were measured in step-scan mode in the 20-80° angular range with a step of 0.02° within the Bragg-Brentano para-focusing geometry. Only the incident beam slit was closed (0.2 mm width), while the diffracted beam slit was left open. The samples were held on microscope slides within a humidity-controlled chamber purposely developed. The scattered intensity was gathered with the Lynxeye XE Energy-Dispersive 1-D detector.

For the assembly of the DSC the different electrodes were sensitized by dipping them in a P1[30] solution (0.3 mM in ACN) for 16 hours. The electrodes were rinsed with ACN to remove the excess of not chemisorbed dye. Optical transmittance of sensitized photocathodes was measured with a double ray spectrometer [UV-2550 by Shimazdu, Kyoto (JP)].

Bare and P1-sensitized photocathodes were assembled in a sandwich configuration with platinised-FTO as counter-electrode. A double layer of Platinum (3D-nano) was screen-printed onto the counter-electrodes. The first layer was dried at 120 °C for 10 min before printing the second one. As the first, the second layer was dried at 120°C in order to burn the solvents. Successively the counter-electrodes were fired at 480 °C in oven for 30 min for the thermal reduction of the Pt precursor[31]. A thermoplastic resin (Surlyn®, from Dupont), was used as spacer and sealant. The electrolyte (Iodolyte-H from Solaronix) was injected inside the two sandwiched electrodes by vacuum backfilling technique through a drilled hole -one for each cell- in the Surlyn® mask. These holes were sealed with a specific UV-curable resin (TB3035B from ThreeBond®).

Photoelectrochemical characterization of the *p*-DSCs consisted in the recording of the JV characteristic curves, incident photon-to-current conversion efficiency (IPCE) spectra and in-light EIS data. All the measurements were recorded with a Sun Simulator AM 1.5G at 1 SUN (Incident Power = 1000 W $m^{-2}$) using a Keithley 2420 as a source-meter in ambient conditions. The light source was calibrated with s SKS1110 sensor (Skye Instruments Ltd).

## RESULTS AND DISCUSSION

Figure 1 shows the voltammograms of bare NiO and NiO_$ZrO_2$_2%, which were recorded within the potential range -0.5 - 1 V *vs* Ag/AgCl at different scan rates (range:10-200 mV $s^{-1}$). In both series of CVs two main peaks are observed: the peak at lower potential corresponds to the reversible solid state oxidation of NiO with occurrence of $Ni^{2+} \rightarrow Ni^{3+} + 1\ e^-$ (named O1); the peak at higher potential is assigned to the formal oxidation of preexisting $Ni^{3+}$ sites into $Ni^{4+}$ (named O2)[32]. The current peak of O1 was more than doubled in going from bare NiO to the sample NiO_$ZrO_2$_2%. Moreover, a sensible variation of the O2/O1 ratio is observed in the compared analysis of NiO and NiO_$ZrO_2$_2% electrodes being the O2 peak less pronounced when the electrode is doped/combined with $ZrO_2$. This combination of findings leads us to suppose that the presence of zirconia as a fine dispersion diminishes the surface concentration of Ni(III) in the *as deposited* sample. Beside the diminution of the portion of defective NiO, i.e. the portion containing Ni(III) sites, the presence of zirconia would favor the relative increase of the surface concentration of Ni(II) sites with respect to bare NiO. The latter statements are going to be verified in a successive study through the adoption of the XPS technique for the speciation of these NiO/$ZrO_2$ nanocomposites. In Table 1, the charge density exchanged during the occurrence of O1 and O2 as well as their relative ratio are reported. The O2/O1 ratio decreases regularly upon increase of $ZrO_2$ content up to the composition NiO_$ZrO_2$_2%. When the $ZrO_2$/NiO ratio becomes higher (samples NiO_$ZrO_2$_5% and NiO_$ZrO_2$_10%), the ratio O2/O1 increases again. This is a consequence of the fact that zirconia should form aggregates at relatively high concentrations thus becoming a

segregated phase, i.e. $ZrO_2$ is not longer homogeneously dispersed in the form of nanoparticles within the NiO nanostructure. In the aggregated state zirconia, i.e. the component representing the passivating and non-electroactive agent of the composite, becomes less efficient in blocking the $Ni^{3+}$ sites. Simultaneously, the presence of $ZrO_2$–based macrostructure on the NiO surface decreases the active surface area of the electrode. In this context the presence of $ZrO_2$–based macrostructure on NiO surface can explain both the detrimental effect on NiO electrochemical activity of the electrode as well as the increase in O2/O1 ratio.

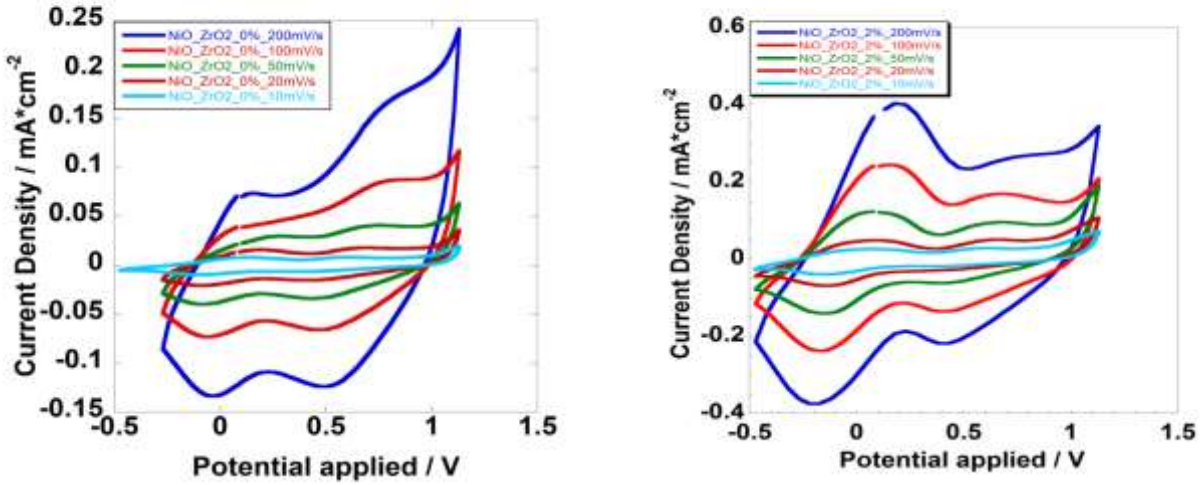


Figure 1. **CVs of** (right) **NiO bare and** (left) **NiO_$ZrO_2$_2% at different scan rates** [**10 mV/s (light blue), 20 mV/s (red), 50 mV/s (green), 100 mV/s (light red) and 200 mV/s (dark blue)**]. **The supporting electrolyte** was **0.1 M $LiClO_4$** in **ACN. CE was a platinum rod and RE is SSE ( +0.220 mV** *vs* **NHE).**

| **Electrode** | O1 peak (mC $cm^{-2}$) | O2 peak (mC $cm^{-2}$) | O2/O1 (%) |
|---|---|---|---|
| NiO | 0.195 | 0.207 | 106.2 |
| NiO_$ZrO_2$_0.1% | 0.206 | 0.178 | 86.4 |
| NiO_$ZrO_2$_1% | 0.461 | 0.144 | 31.2 |
| NiO_$ZrO_2$_2% | 0.990 | 0.200 | 20.2 |
| NiO_$ZrO_2$_5% | 0.686 | 0.162 | 23.3 |
| NiO_$ZrO_2$_10% | 0.096 | 0.033 | 34.3 |

**Table 1.** Charge density exchanged during the processes identified as O1 and O2 and relative ratio.

From Table 1, it could be evidenced that NiO_$ZrO_2$_2% showed both the better electrochemical activity, i.e. the higher value of exchanged charge, and the relatively lower extent of $Ni^{3+}$ in the sample being this characteristic associated with the lower O2/O1 ratio. Because of that, sample NiO_$ZrO_2$_2% appeared as the most suitable electrode to be employed as photocathode in a *p*-DSC[33].

For the detection of the eventual presence of these $ZrO_2$–based macrostructures we performed combined SEM-EDX measurements. SEM (Figure 2) evidenced all samples possessed a quite open morphology with a lot of nanometer size voids: such a morphological feature is essential to assure a sufficiently high dye-loading for DSC purposes. The presence of $ZrO_2$ macrostructures was detected in all samples. For the determination of the actual chemical nature of the macrostructures we analyzed the elemental distribution on the electrode surface with Energy Dispersive X-ray (EDX, figure 3) spectroscopy. The analysis concerned the search of the elements Ni, O and Zr. The

eventual presence of Sn from FTO substrate was also checked to evaluate the porosity of the screen-printed electrodes. Are here shown the SEM and EDX images of NiO, NiO_$ZrO_2$_2% and NiO_$ZrO_2$_5%. Additional images have been collected in the supporting information (Figures ESI1-ESI4).

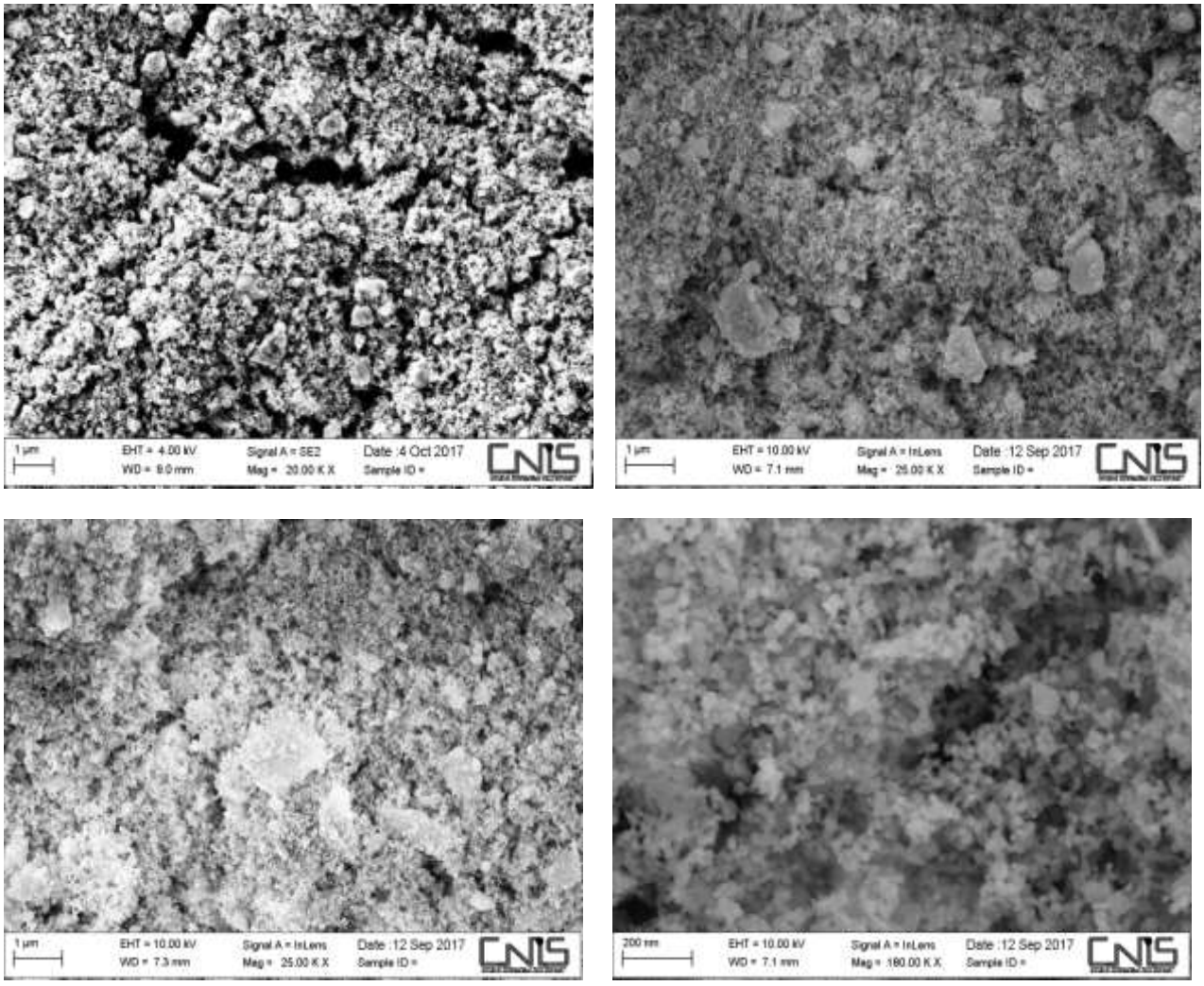


**Figure 2.** SEM image of the NiO electrodes differing for the amount of $ZrO_2$: (top left) NiO; (top right) NiO_$ZrO_2$_2% and (bottom left) NiO_$ZrO_2$_10%. A magnification of NiO_$ZrO_2$_2% has been shown (bottom right) to evidence the dispersion of $ZrO_2$ NPs onto the NiO surface.

By the comparison of images in Figure 2 and ESIX, one can see that a $ZrO_2$/NiO molar ratio higher than 2% leads to the growth of some macrostructures. The latter feature became more evident in NiO_$ZrO_2$_10%. Interestingly, the presence of nanoparticles randomly dispersed onto the electrode surface was evidenced too with EDX spectroscopy. EDX confirmed also that the $ZrO_2$ macrostructures were formed by the aggregation of $ZrO_2$ NPs in the samples with the largest concentration of zirconia. As shown in figure ESIX, a concentration of Zr and a lower amount of Ni was revealed in the analyzed area. Moreover, this structure is not porous since the signal of Sn could not be detected. The presence of superficial Zr could not be found in NiO_$ZrO_2$_0.1% (Figure ESI1) because of the too high dispersion of $ZrO_2$ NPs, which is below the sensitivity of the EDX instrument (0.065 mmol per unit area). The signal of Sn was detected for all nanocomposites with molar content of Zr smaller than 10% (See ESI5).

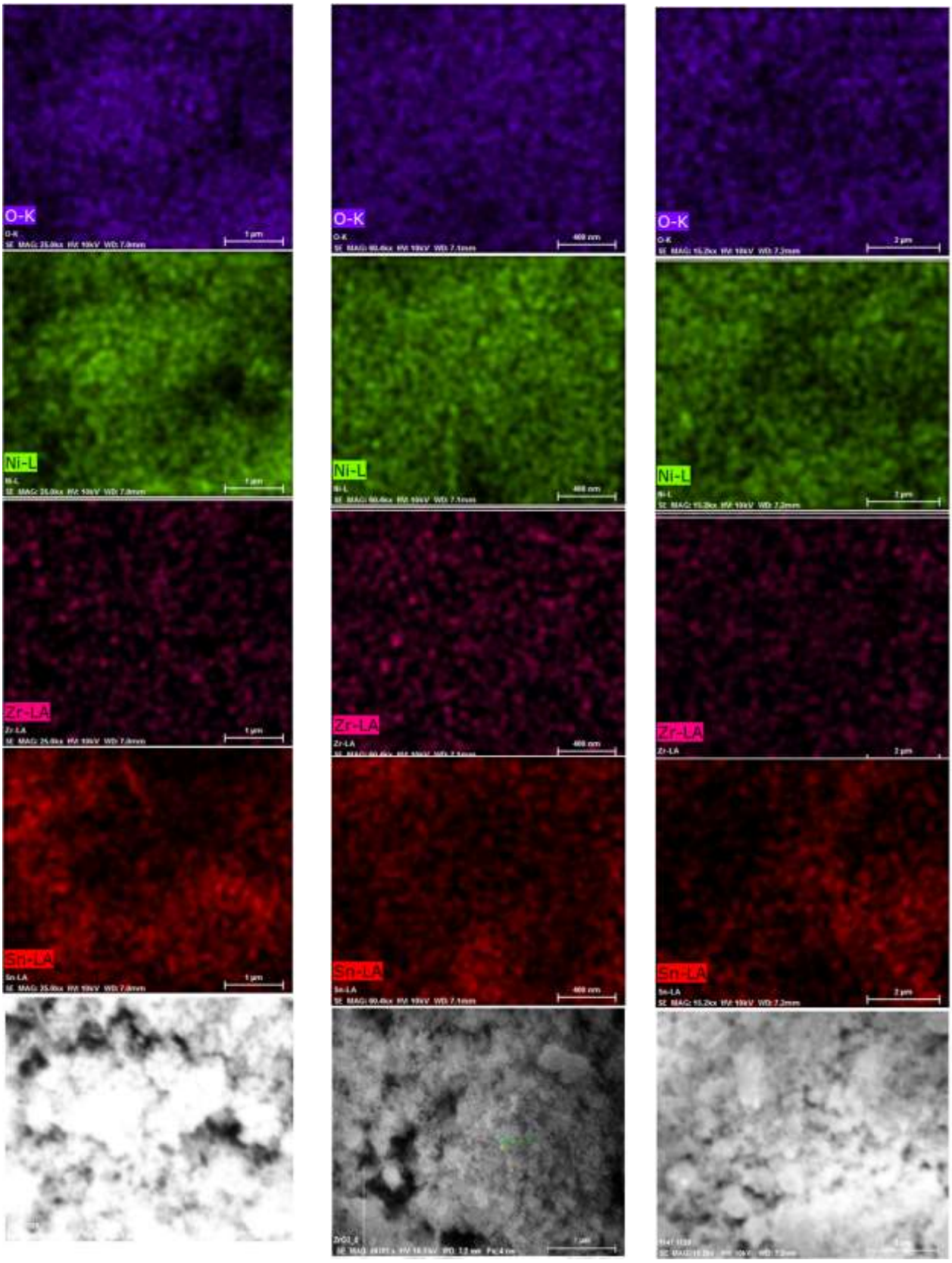


**Figure 3.** EDX images of (left column) NiO_$ZrO_2$_1%, (middle column) NiO_$ZrO_2$_2% and (right column) NiO_$ZrO_2$_5%. The surface distribution of different elements has been marked with different colors: violet-blue = O (first row of images); green = Ni (second row of images); pink = Zr (third row of images); red = Sn (fourth row of images). The bottom row represents the morphology of the three different samples of nanocomposites here considered.

The *Tauc's plot* was employed to determine the optical band gap of not sensitized electrodes upon variation of zirconia content (Figure 4).

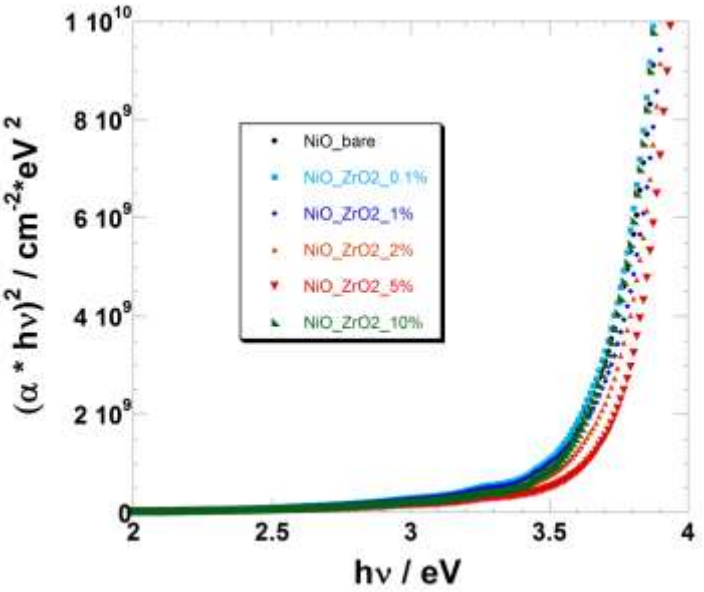


**Figure 4.** Tauc's plot for the extrapolation of the optical bandgap in the different nanocomposites of NiO and $ZrO_2$. Black circles: NiO; light blue squares: NiO_$ZrO_2$_0.1%; dark blue diamonds: NiO_$ZrO_2$_1%; orange triangles: NiO_$ZrO_2$_2%; red triangles: NiO_$ZrO_2$_5%; green triangles: NiO_$ZrO_2$_10%.

In the present case, the bandgap $E_g$ for this series of nanocomposites tends to increase monotonically on going from NiO to NiO_$ZrO_2$_5% whereas the bandgap of NiO_$ZrO_2$_10% is very similar to the one of NiO. More precisely, the calculated bandgap is 3.62, 3.61, 3.68, 3.71, 3.75 and 3.63 for NiO, NiO_$ZrO_2$_0.1%, NiO_$ZrO_2$_1%, NiO_$ZrO_2$_2%, NiO_$ZrO_2$_5% and NiO_$ZrO_2$_10%, respectively. The blue-shifted $E_g$ of the $ZrO_2$ /NiO electrode with respect to NiO leads to more transparent films of the nanocomposites with respect to NiO in the visible range. A larger number of defects in the lattice corresponds to a system with a tighter the optical band gap.

Electrochemical impedance spectra were recorded in a three-electrode cell configuration in dark condition in order to avoid any modification induced by the eventual photoactivity of NiO working electrode. The applied potential ranged in the interval -0.2 - 1.1 V (*vs* Ag/AgCl) (Figure 5). Experimental data have been fitted with the equivalent circuit depicted in Figure ESI5: the first element simulates charge-transfer phenomena occurring at the electrode/electrolyte interface whilst the second accounts for the charge transport through the electrode with its characteristic charge transport resistance and capacitance. In the present context, we focus our attention and discuss mainly the former type of phenomenon, i.e. interfacial charge transfer since this represents the process at the basis of recombination in the actual *p*-DSC device and constitutes the problem which is here tackled through the introduction of nanocomposites of electroactive NiO and electrochemically inert $ZrO_2$. The electrolyte composition in the experiments of electrochemical impedance is the same as the one employed in the experiments of cyclic voltammetry.

In Table 2 $R_{CT}$ represents the charge transfer (CT) resistance at the electrolyte/electrode interface, $C_{INTER}$ is the double layer capacitance whereas $C_{electrode}$ is the capacitance of the electrode layer. EIS data evidenced that $R_{CT}$ diminishes with the applied potential irrespective of the amount of zirconia in the electrode. This is expected since the increase of the applied potential is accompanied by the concomitant increase of the number of holes, i.e. the mobile charged species that are injected

electrochemically in the film of NiO during its oxidation. Beside the improvement of the charge transfer properties these holes contribute to the double layer capacitance $C_{INTER}$ at electrode/electrolyte interface and to the capacitance $C_{electrode}$ of the electrode bulk. When CT is relatively fast it promotes the formation of a diffuse double layer instead of a compact one. The $R_{CT}$ values decrease sharply when the applied potential approaches the values of NiO redox processes, i.e. between 0 and 0.25 V and between 0.5 and 0.7 V for $Ni^{2+}$ -> $Ni^{3+}$ and $Ni^{3+}$ -> $Ni^{4+}$ reactions, respectively. A similar behaviour has been already reported for NiO when is polarized in aqueous electrolytes[34]. Among the various formulations of the nanocomposites in the pristine state, the system NiO_$ZrO_2$_2% showed the lowest $R_{CT}$ (2218 Ω), and the largest values of the capacitive terms $C_{electrode}$ and $C_{INTER}$. These findings denote the existence of a quite defective material with a relatively high number of native charges in starting NiO_$ZrO_2$_2%. Upon completion of the oxidation processes ($E_{appl}$ = 1.10 V vs Ag/AgCl) NiO_$ZrO_2$_2% presented also the largest value of $R_{CT}$ (twice the value of bare NiO one): this is an indication of the stronger tendency of this particularly formulation of nanocomposite to suppress efficaciously recombination at the electrode/electrolyte interface with respect to the other combinations.

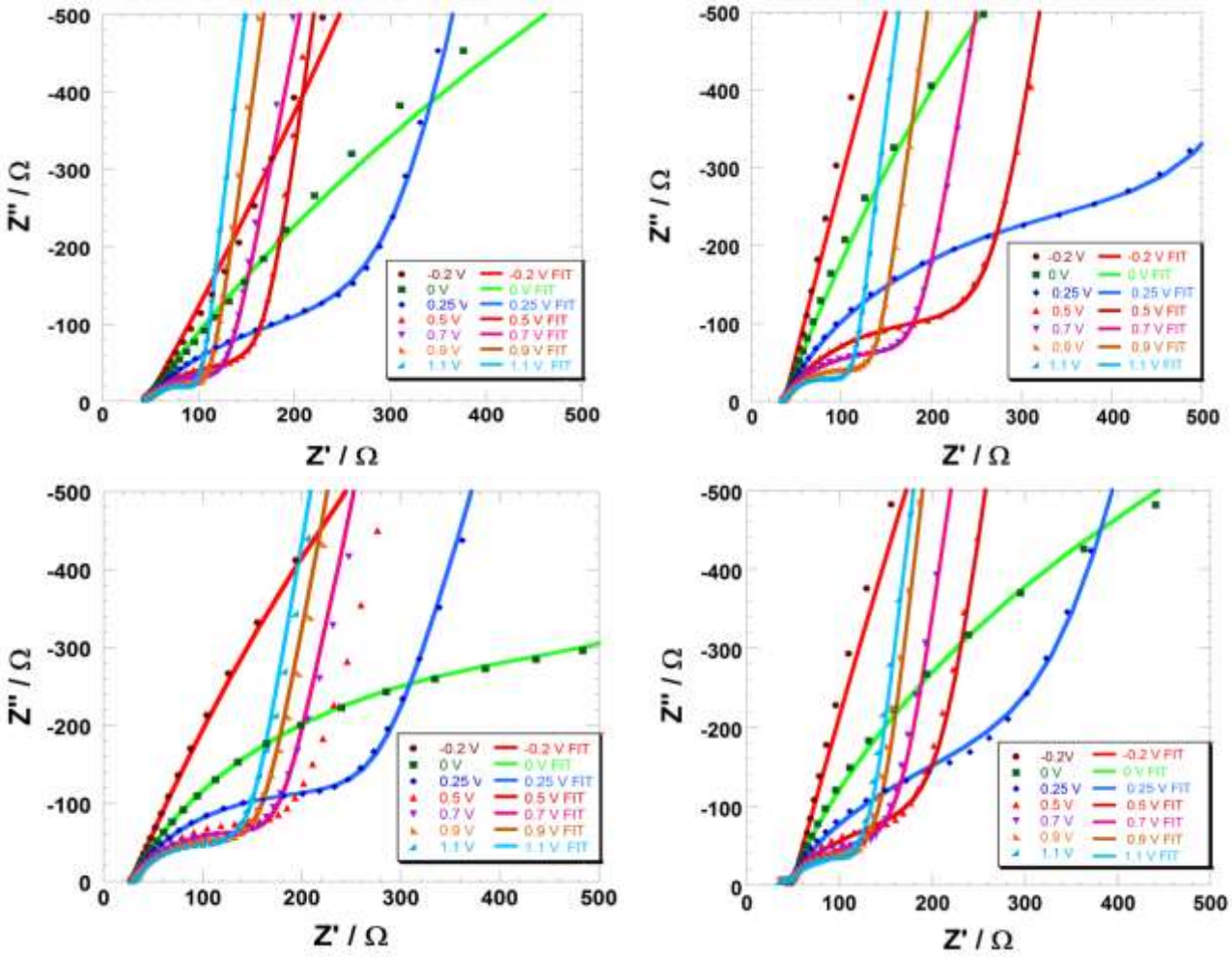


**Figure 5.** EIS data of (top left) NiO bare, (top right) NiO_$ZrO_2$_1%, (bottom left) NiO_$ZrO_2$_2% and (bottom right) NiO_$ZrO_2$_10% at different applied potential: -0.20 (dark red circles), 0.00 (dark green squares), 0.25 (dark blue diamonds), 0.50 (red triangles), 0.70 (purple triangles), 0.90 (orange triangles) and 1.10 V *vs* Ag/AgCl (light blue triangles). The fittings have been reported as full lines.

| | E / V *vs* Ag/AgCl | -0.20 | 0.00 | 0.25 | 0.50 | 0.70 | 0.90 | 1.10 |
|---|---|---|---|---|---|---|---|---|
| NiO | $R_{CT}$ / Ω | 3715 | 1942 | 284 | 131 | 88 | 71 | 62 |
| | $C_{INTER}$ / μF | 33.2 | 28.6 | 24.4 | 16.2 | 11.9 | 10.2 | 9.2 |
| | $C_{electrode}$ / μF | 53.8 | 178.2 | 198.5 | 212.1 | 225.2 | 236.7 | 239.8 |
| NiO_$ZrO_2$_0.1% | $R_{CT}$ / Ω | 3134 | 707 | 312 | 198 | 131 | 99 | 84 |
| | $C_{INTER}$ / μF | 37.3 | 31.7 | 22.3 | 20.7 | 14.1 | 13.5 | 12.4 |
| | $C_{electrode}$ / μF | 55.3 | 184.4 | 218.8 | 232.2 | 242.6 | 252.9 | 254.6 |
| NiO_$ZrO_2$_1% | $R_{CT}$ / Ω | 2540 | 635 | 328 | 237 | 151 | 126 | 102 |
| | $C_{INTER}$ / μF | 43.8 | 35.9 | 26.1 | 21.3 | 17.9 | 15.3 | 13.6 |
| | $C_{electrode}$ / μF | 65.1 | 223.2 | 293.2 | 301.2 | 332.9 | 336.5 | 362.8 |
| NiO_$ZrO_2$_2% | $R_{CT}$ / Ω | 2218 | 593 | 248 | 179 | 148 | 130 | 119 |
| | $C_{INTER}$ / μF | 49.7 | 33.7 | 26.5 | 20.4 | 17.6 | 15.6 | 14.8 |
| | $C_{electrode}$ / μF | 170.1 | 332.2 | 383.3 | 393.8 | 436.4 | 446.0 | 470.7 |
| NiO_$ZrO_2$_5% | $R_{CT}$ / Ω | 2649 | 741 | 346 | 264 | 164 | 133 | 112 |
| | $C_{INTER}$ / μF | 47.9 | 36.0 | 26.5 | 19.7 | 17.3 | 15.1 | 13.8 |
| | $C_{electrode}$ / μF | 132.0 | 248.9 | 340.8 | 342.8 | 367.9 | 384.6 | 402.3 |
| NiO_$ZrO_2$_10% | $R_{CT}$ / Ω | 4135 | 1002 | 422 | 280 | 136 | 117 | 108 |
| | $C_{INTER}$ / μF | 46.6 | 31.7 | 23.7 | 17.2 | 14.4 | 12.6 | 11.7 |
| | $C_{electrode}$ / μF | 72.2 | 191.8 | 198.6 | 204.6 | 228.9 | 230.9 | 236.9 |

**Table 2.** Electric parameters derived from the fit of experimental impedance spectra. The errors on the fitting parameters are less than 3%.

In order to check the crystallographic structure of our modified samples and the eventual arising of some NiO/ZrO2 mixed phase, we performed X-Ray Diffraction measurements. The results have been reported in figure 6: as one can see, the XRD spectrum of bare NiO (JCPDS card No. #47-1049) shows one main peak corresponding to the 111 plane (at 37.2°) and a smaller peak at 75.1° corresponding to the 311 plane. All the peak indexed with * arising from the FTO employed as substrate[35]. The addition of $ZrO_2$ NPs leads to a slight modification of the XRD pattern: two small peaks could be evidenced at 42.8° and 62.5° ascribable to the 200 and 220 plane of cubic NiO (JCPDS card No. #47-1049), respectively. Furthermore, there is not any evidence of peak due to $ZrO_2$ or NiO/$ZrO_2$ mixed phases. The XRD pattern of monoclinic $ZrO_2$ usually presents two main peaks at 28.1° (110) and 31.4° (111), JCPDS card No. #78-1807, whereas the spectrum of tetragonal zirconia is composed by three main peaks centred at 30.2° (101), 50.2° (112) and 60.2° (211), JCPDS card No. #79-1769. The absence of any crystallographic peak of $ZrO_2$ is ascribable to the homogenous dispersion of the nanoparticles (figure 3) that not allow the occurrence of large ZrO2 crystallographic domains. Therefore, the effect of the addition of $ZrO_2$ results in the growth of the NiO matrix in additional crystalline planes. More interestingly, the rise of NiO/$ZrO_2$ mixed phase could be completely ruled out.

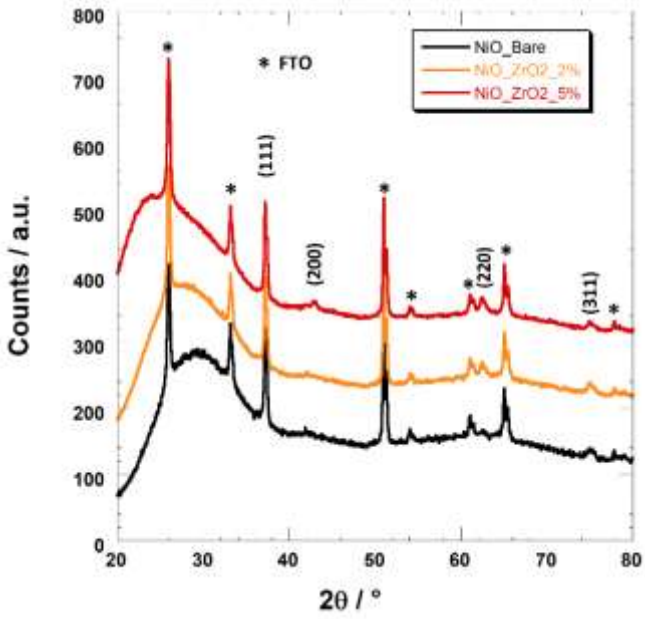


**Figure 6.** XRD spectra of bare NiO (black line), NiO_ZrO2_2% (orange line) and NiO_ZrO2_5% (red line) films. The peak due to the presence of crystalline NiO are indexed by the name of the corresponding plane. *-indexed peak refers to FTO substrate.

The *JV* curves of the *p*-DSCs with the six formulations here considered have been recorded for both pristine and P1-sensitized electrodes to stress eventual changes in the operating features of the NiO-based electrode after sensitization. When dye is not loaded onto the NiO surface, the only accessible pathway to produce photocurrent is the excitation of an electron from the VB of NiO to its CB at the approximate wavelength of excitation $\lambda_{exc} \approx 320$ nm. To reduce the current losses due to recombination phenomena, $Ni^{3+}$ sites should be inaccessible to the reducing species that are present in solution: the implementation of $ZrO_2$ NPs avoids that the surface of nickel oxide with its recombination defects is fully exposed to the electrolyte. The practical effect of the introduction of $ZrO_2$ NPs is the increase in the powered photocurrent: +123% on going from pristine NiO to NiO_$ZrO_2$_2% (Figure 7 and Table 3) accounting for a huge decrease in recombination phenomena. NiO and NiO_$ZrO_2$_2% produced a photocurrent of 0.448 mA*$cm^{-2}$ and 0.994 mA $cm^{-2}$ , respectively. The trend of photocurrent is not monotonic: it reached its maximum when $ZrO_2$ to NiO have a molar ratio of 2% and it decreased for NiO_$ZrO_2$_5% and NiO_$ZrO_2$_10% ($J_{SC}$ = 0.747 and 0.414 mA $cm^{-2}$, respectively). This trend is in accordance with the CV and EIS data (*vide supra*). Such a combination of findings shows how revealing is the analysis of the electrochemical properties in case of nanostructured NiO electrodes for the successive evaluation of their photoelectrochemical performance. When compared to sole NiO, the sample of NiO_$ZrO_2$_0.1% does not show any significant difference in terms of electrochemical and photoelectrochemical behavior due to the fact that zirconia NPs are too dispersed to effectively influence the (photo)electrochemical properties of the corresponding nanocomposite electrode. NiO_$ZrO_2$_1%, NiO_$ZrO_2$_2% and NiO_$ZrO_2$_5% manifested similar electrochemical behavior and displayed similar morphologies. In case of NiO_$ZrO_2$_1% such a concentration of $ZrO_2$ does not allow a good dispersion of the nanoparticles throughout the NiO film whereas molar percentage values higher than 2% causes the formation of pure $ZrO_2$ macrostructure that can prevent the exposure of the $Ni^{3+}$ sites. Among the doped electrode NiO_ZrO2_10% showed the worst performance: the electrode mainly suffered for an extremely low Fill Factor (FF ≈ 25%). Such a result could be ascribed to the presence of large aggregates of zirconia that produce as main effect the inhibition of the process of

photoinjection rather than preventing recombination. Moreover, the electrode formulation NiO_$ZrO_2$_5% showed a relatively low FF (≈ 28%) too. Open circuit potential ($V_{OC}$) values ranged from 78 to 85 mV without showing any clear trend with the amount of dispersed zirconia.

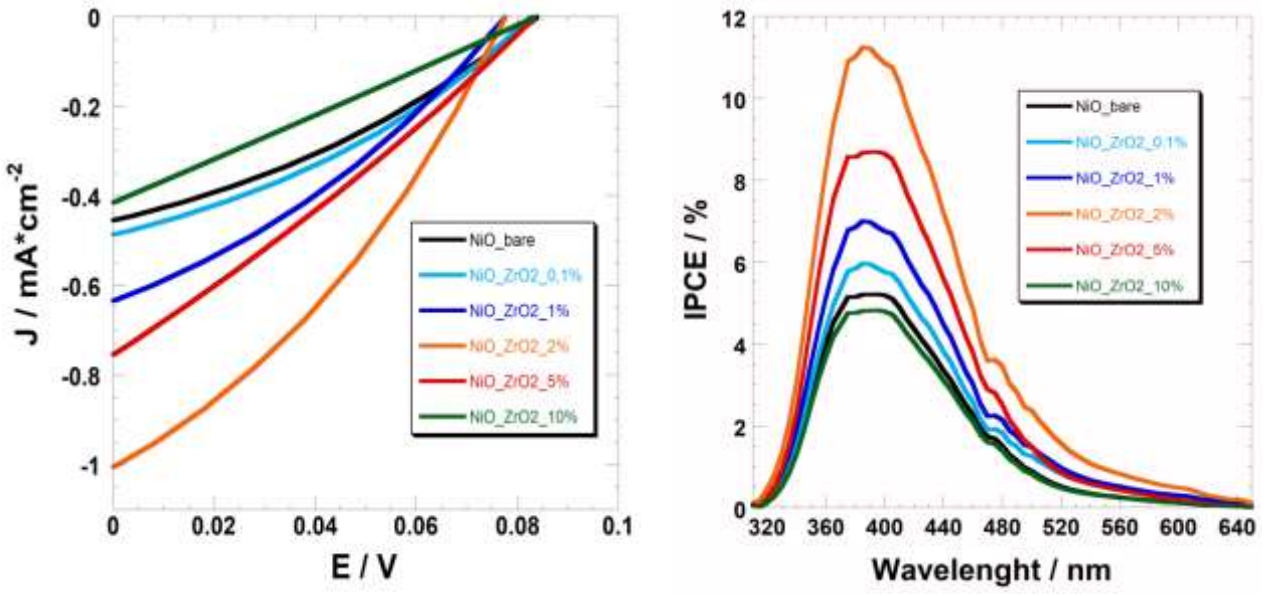


**Figure 7.** (Left) *JV* curves and (right) IPCE spectra of the p-DSCs employing bare electrodes with different doping degree: 0% (black), 0.1% (light blue), 1% (dark blue), 2% (orange), 5% (red) and 10% (green).

By definition the IPCE (Incident Photo-to-current Conversion Efficiency) is the ratio of the number of collected carriers to the number of all the incident photons on the device active area at a given wavelength. The differences in the spectra reported in figure 7 evidence that the probability with which the photoinjected holes reach the current collector ($\eta_{tr}$) varies with the content of zirconia and follows the trend of the photocurrent, i.e. the higher the photocurrent powered by the device, the higher the maximum of the IPCE spectra. Some little shifts of the wavelength corresponding to IPCE maximum are expected for the different electrodes due to the blue-shift of the optical bandgap introduced by the presence of zirconia, as previously outlined.

P1 was the sensitizer of our *p*-DSCs[36] (sensitization conditions: 16 hours in a 0.3 mM solution of the dye in ACN). NiO_$ZrO_2$_10% has been excluded from the analyses because of its poor electrochemical and photoelectrochemical performance. Upon sensitization the enhancement of the photocurrent is clear in going from NiO to NiO_$ZrO_2$_2%. Yet the magnitude of such an increase is lower compared to the corresponding increase when un-sensitized electrodes are employed (+ 46% *vs* +123%, respectively). This difference was mainly due to the presence of the sensitizer: the dye partially acts as a passivating agent by reducing the free $Ni^{3+}$ sites that represent the actual sites of anchoring. Some of the $Ni^{3+}$ sites are actively involved in binding P1 onto the NiO surface, whereas other are simply covered as a consequence of the steric hindrance of the organic molecule. $J_{SC}$ values varied from 1.447 mA $cm^{-2}$ to 2.037 mA $cm^{-2}$ in passing from bare NiO to NiO_ $ZrO_2$_0.020. To our knowledge the efficiency value of 0.088% here obtained with P1-sensitized NiO_$ZrO_2$_0.020. is the highest reported for a P1-sensitized screen-printed NiO electrode without the integration of a NiO compact layer[37,38]. NiO_$ZrO_2$_0.1% and NiO_$ZrO_2$_1% have shown quite similar performances (1.611 and 1.690 mA $cm^{-2}$ of short circuit current density, respectively) but far from the record value.

| | Dye | $J_{SC}$/ mA*cm$^{-2}$ | $V_{OC}$ / mV | FF / % | η / % | Dye Loading / $10^{8}$*mmol*cm$^{-2}$ |
|---|---|---|---|---|---|---|
| **NiO** | **-** | **0.448 ± 0.012** | **83 ± 2** | **33.8 ± 0.9** | **0.012** | **-** |
| **NiO_ZrO$_2$_0.001** | **-** | **0.480 ± 0.020** | **83 ± 2** | **34.1 ± 0.7** | **0.014** | **-** |
| **NiO_ZrO$_2$_0.010** | **-** | **0.618 ± 0.023** | **78 ± 1** | **33.2 ± 0.7** | **0.016** | **-** |
| **NiO_ZrO$_2$_0.020** | **-** | **0.994 ± 0.033** | **78 ± 2** | **33.7 ± 0.6** | **0.026** | **-** |
| **NiO_ZrO$_2$_0.053** | **-** | **0.747 ± 0.028** | **75 ± 3** | **27.9 ± 0.9** | **0.017** | **-** |
| **NiO_ZrO$_2$_0.111** | **-** | **0.414 ± 0.056** | **84 ± 3** | **25.3 ± 0.8** | **0.009** | **-** |
| **NiO** | **P1** | **1.447 ± 0.120** | **129 ± 2** | **32.5 ± 0.6** | **0.060** | **3.19 ± 0.62** |
| **NiO_ZrO$_2$_0.001** | **P1** | **1.611 ± 0.089** | **130 ± 2** | **32.4 ± 0.5** | **0.068** | **3.16 ± 0.52** |
| **NiO_ZrO$_2$_0.010** | **P1** | **1.690 ± 0.103** | **130 ± 3** | **34.4 ± 0.5** | **0.075** | **3.27 ± 0.39** |
| **NiO_ZrO$_2$_0.020** | **P1** | **2.037 ± 0.095** | **129 ± 2** | **33.6 ± 0.6** | **0.088** | **3.22 ± 0.41** |
| **NiO_ZrO$_2$_0.053** | **P1** | **1.313 ± 0.063** | **126 ± 1** | **30.5 ± 0.3** | **0.050** | **2.65 ± 0.53** |
| **NiO_ZrO$_2$_0.111** | **P1** | **-** | **-** | **-** | **-** | **-** |

**Table 3.** Photoelectrochemical parameters of the *p*-DSCs with the differently doped $ZrO_2$-NiO nanocomposite photoelectrodes. The reported values are obtained from averaging the performances of five devices. The errors on the efficiency values are lower than 0.001 and have not been reported.

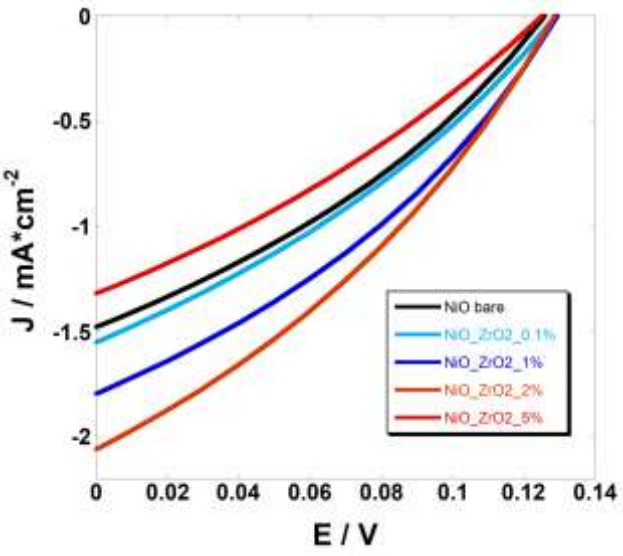


**Figure 8.** *JV* curves of the complete devices built up with P1-sensitized electrodes with different doping degree: 0% (black), 0.1% (light blue), 1% (dark blue), 2% (orange) and 5% (red).

NiO_ZrO$_2$_5% displayed the worst performance in terms of current density and open circuit voltage. The lower values of $J_{SC}$, $V_{oc}$ and FF are mainly due to an insufficient dye-loading (see Table 3): zirconia macrostructures, even if they are not as extended as in case of NiO_ZrO$_2$_10% (see SEM pictures in Figure 2), seem to prevent the full penetration of the sensitizer throughout the porous structure of the electrode with consequent insufficient dye-loading. Similar to not sensitized devices, no substantial variations of $V_{OC}$ could be observed. The highest values of fill factor (34.4% and 33.6%), have been reported when the fraction of $ZrO_2$ are 1% and 2%. This evidence confirms the optimal dispersion of zirconia NPs in the fraction range of 1-2 % as already outlined by the electrochemical measurements. IPCE spectra of the P1-sensitized devices (Figure 9), confirmed the trend shown by *JV* curves.

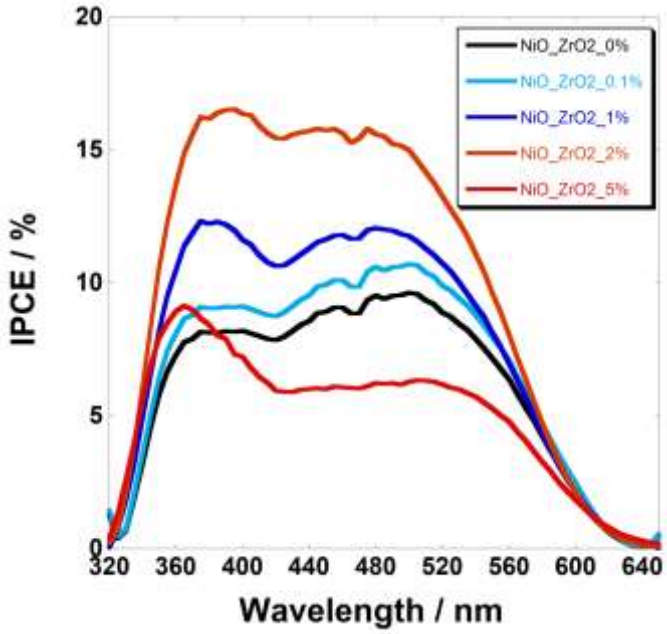


**Figure 9.** IPCE spectra of the complete devices built up with P1-sensitized electrodes with different doping degree: 0% (black), 0.1% (light blue), 1% (dark blue), 2% (orange) and 5% (red).

The different performances of the *p*-DSCs differing for the composition of the nanocomposite electrodes could be ascribed to a minimization of the recombination reactions involving the reduced species in the electrolyte, i.e. $I^-$, and the surface localized holes in the NiO electrode. The similar values of dye loading and bandgap for the series of electrodes here considered indicate that the kinetics of charge injection is not sensibly altered by the fraction of zirconium oxide. The electrochemical impedance spectra of the different photelectrochemical cells are presented in Figure 9. For sake of simplicity the impedance spectrum of the DSC with NiO_$ZrO_2$_0.1% photocathode is not shown due to the similarity with the spectrum of the cell having sole NiO photocathode.

The electric parameters reported in Table 4 could be extracted from experimental data when the equivalent circuit[28] of the inset of Figure 10 is adopted as model. In this model $R_s$ is the resistance of all the external elements. It should be constant within the experimental error. $R_{CE}$ is the resistance of charge transfer through the electrolyte/counter electrode interface and corresponds to the process of oxidation of the reduced species of the redox shuttle (i.e. $I^-$) at Pt electrode. $C_{CE}$ is the capacitance at the electrolyte/counter electrode interface. The following circuital elements have been defined in the transmission line element adapted by Bisquert to analyze the impedance response of *n*-type DSCs [39] and successfully employed for the analysis of the impedance spectra of *p*-type DSCs[28]:

- $R_t$ is the (transport) resistance of the electronic charge carriers, i.e the holes, to traverse the NiO electrode and reach the FTO back contact (charge collector).
- $R_{rec}$ is the resistance of recombination the charge carriers experience after photogeneration. Patterns of recombination can be due either to the recombination of the excited/oxidized dye with the hole or to the recombination of the photogenerated hole with a reducing species in the electrolyte, namely $I^-$.
- $C_\mu$ is the (chemical) capacitance of the NiO-based photocathode and is related to the content of charge that is present inside the illuminated photocathode.

The employment of the transmission line element is consistent with the mesoporous nature of the photocathodes. The pure capacitive elements are here replaced with the CPE (constant phase

element) that allows an easier fit of the experimental data without influencing the reliability of the obtained parameters. The actual capacitance ($C_{real}$) could be calculated applying the following equation:

$$C_{real} = \frac{(C_{CPE} * R)^{\left(\frac{1}{n}\right)}}{R}$$

in which $C_{CPE}$ and *n* are the two parameters describing the capacitive properties of the CPE element whilst R is the value of the resistance associated to CPE. If *n* is equal to 1, the CPE acts a pure capacitance.

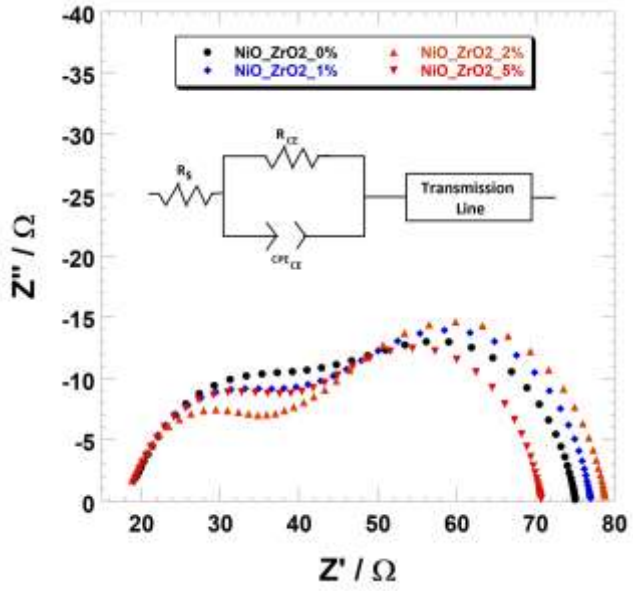


**Figure 10.** EIS spectra of the complete devices built up with P1-sensitized electrodes differing for the fraction of zirconia dopant: 0% (black dots), 1% (dark blue diamonds), 2% (orange triangles) and 5% (red triangles). In the inset, the equivalent circuit employed for the experimental data interpolation is reported.

The determination of these electrical parameters allows the direct calculation of the following microscopic parameters:

- $\tau_h$ (= $R_t$ * $C_\mu$), i.e. the time the photoinjected holes take to reach the FTO charge collector;
- $\tau_{rec}$ (= $R_{rec}$ * $C_\mu$), i.e. the holes lifetime that corresponds to the time the photoinjected holes spend before undergoing any type of recombination process;
- $L_h$ [= $l$ $(R_t/R_{rec})^{1/2}$, where $l$ is the nominal film thickness] is the mean free path of the photoinjected holes before being involved in recombination reactions;
- $D_h$ (=$L_h^2$ /$\tau_h$) is the average diffusion coefficient of the photoinjected holes through the photocathode.

The values of both $R_{CE}$ and $C_{CE}$ did not vary considerably with the concentration of $ZrO_2$ NPs in the nanocomposite electrode. The modification in electronic and photoelectronic properties of the working photoelectrode do not influence the kinetics of charge transfer processes at the counter-electrode.

In the *p*-DSCs the value of $R_t$ decreased with the increase of $ZrO_2$ molar content in the photocathode in agreement with the ameliorated electronic transport properties of the NiO electrode

due to the controlled doping with zirconia when the three-electrode cell was analyzed. The presence of zirconia NPs onto the NiO surface reduces the number of free trap sites (i.e. $Ni^{3+}$ surface located sites) which contribute to the chemical capacitance of the electrode. This is proved by the higher value of $C_\mu$ reported for NiO_$ZrO_2$_1% and NiO_$ZrO_2$_2% (101 μF and 115 μF, respectively) compared to the un-doped NiO electrode (89 μF). The relatively low value of chemical capacitance (i.e. 97 μF) recorded for NiO_$ZrO_2$_5% is probably due to the insufficient dye loading that prevents the photoinjection of a high number of carriers. The low value of $R_{rec}$ for the NiO_$ZrO_2$_5% electrode is associated with a relatively low amount of dye. Both un-doped NiO and NiO_ $ZrO_2$_5% electrode showed the lowest $R_{rec}$ values (56.3 Ω and 57.3 Ω, respectively) while NiO_$ZrO_2$_1% with 63.8 Ω and NiO_$ZrO_2$_2% with 70.3 Ω gave the best performing cells in combination with the higher resistance of recombination (see *JV* curves in Figure 7). The analysis of the data showed a linear correlation between $R_{rec}$ and $J_{SC}$: the higher the former the higher the latter. Such a linear correlation does not hold when $\eta$ is correlated to $R_{rec}$ (and $J_{SC}$). The values of $\tau_{rec}$ followed the same trend of $R_{rec}$. A remarkably long time of recombination of 8.1 ms for the charge carriers diffusing through NiO_$ZrO_2$_2% has been found in combination with long diffusion length (3.7 μm) and high diffusion coefficient (5.7 $*10^{-5}$ $cm^2$ $s^{-1}$). This is a consequence of the fact that the photoinjected holes have a longer mean free path and a higher rate of diffusion throughout the NiO film in presence of zirconia nanoparticles with respect to undoped NiO. The $Ni^{3+}$ trap states are expected to be masked and eventually annihilated upon addition of zirconia nanoparticles. For the confirmation of the latter statement the analysis of the surface with XPS will be necessary and is planned in a successive study. The photoelectrode formulation NiO_ $ZrO_2$_5% presented a low value of $\tau_{rec}$, as well as the lowest value of $\tau_h$ within the series of the electrodes. It is expected that such a content of zirconia prevents the homogeneous sensitization of the anchoring sites of NiO, which also behave as trapping species. Such sites in the not sensitized state contribute to lower the hole diffusion time with the consequent attainment of high values of $D_h$ (Table 4).

| $ZrO_2$ (%) | 0 | 1 | 2 | 5 |
|---|---|---|---|---|
| $R_{CE}$ (Ω) | 13.0 ± 0.1 | 13.3 ± 0.2 | 13.0 ± 0.1 | 12.8 ± 0.1 |
| $C_{CE}$ (μF) | 12.7 ± 0.3 | 13.1 ± 0.2 | 12.4 ± 0.2 | 12.3 ± 0.1 |
| $R_t$ (Ω) | 27.3 ± 0.5 | 23.0 ± 0.4 | 20.8 ± 0.2 | 18.6 ± 0.5 |
| $R_{rec}$ (Ω) | 56.3 ± 0.5 | 63.8 ± 0.8 | 70.3 ± 0.7 | 57.3 ± 0.8 |
| $C_\mu$ (μF) | 89 ± 3 | 101 ± 3 | 115 ± 4 | 97 ± 3 |
| $\tau_h$ (ms) | 2.4 ± 0.1 | 2.3 ± 0.1 | 2.3 ± 0.1 | 1.8 ± 0.1 |
| $\tau_{rec}$ (ms) | 5.0 ± 0.1 | 6.4 ± 0.2 | 8.1 ± 0.1 | 5.6 ± 0.1 |
| $L_h$ (μm) | 2.9 ± 0.3 | 3.3 ± 0.2 | 3.7 ± 0.2 | 3.5 ± 0.2 |
| $D_h$ ($cm^2/s$) $*10^{-5}$ | 3.4 ± 0.1 | 4.8 ± 0.2 | 5.7 ± 0.2 | 6.9 ± 0.3 |

**Table 4.** Microscopic parameters with the relative errors as determined by the interpolation of EIS spectra of Figure 9. The reported values are averaged considering the measurements conducted on five different cells with the photoelectrodes from the same batch.

Treatments like the deposition of a blocking layer between the FTO and the photocathode or the post-sintering surface modification of NiO based electrodes are expected to further enhance the performance of *p*-DSCs. For this reason, further experiments in the direction of the modification of the photocathode with inclusion of a blocking compact layer and consideration of post deposition treatments will be planned. The main motivation of the conduction of this type of studies is the implementation of the best performing photocathodes in tandem DSCs when comparable current

densities and efficiencies are achieved at the corresponding photoelectrodes of *p*- and *n*-type devices.

## CONCLUSIONS

The nanocomposites obtained from the sintering of nanoparticles (NPs) of nickel oxide (NiO) and zirconia ($ZrO_2$) have been employed as photocathodes of *p*-type dye-sensitized solar cells (*p*-DSCs), P1 being the sensitizer. NiO represented the component in large excess whereas $ZrO_2$ constituted the doping species of the nanocomposite with a percentage of less than 10%. Nano-dispersed $ZrO_2$ minimized recombination phenomena at the electrode/electrolyte interface of the *p*-DSC when the redox shuttle was the couple $I^-/I_3^-$. The best performance of the photoelectrochemical cell was obtained with the electrode having the 2% of $ZrO_2$ in the NiO matrix. This enhancement (due to the addition a controlled amount of ZrO2 NPs) was firstly ascribed to a minimization of the recombination phenomena occurring at the electrode/dye/electrolyte interface. Electrochemical impedance measurements were employed to prove this hypothesis: recombination resistance was improved by 25% (from 56.3 to 70.3 Ω); additionally, hole transport resistance was reduced to 20.8 Ω (from 27.3 Ω of bare NiO). These evidences lead to slower recombination time, faster hole transport, longer hole diffusion length and higher diffusion coefficient. The efficiencies of the *p*-DSCs with NiO/ $ZrO_2$ nanocomposites were 123% and 48% higher than un-doped NiO for the bare and sensitized electrode, respectively. SEM-EDX experiments have been performed to visualize the pattern of dispersion of $ZrO_2$ NPs in the NiO matrix. The values of 0.1 and 1% of zirconia do not assure a uniform dispersion. When the concentration of zirconia was higher than 5%, the NPs merged to form macrostructures. This phenomenon of $ZrO_2$ NPs aggregation on the electrode surface prevented surface passivation and efficient dye-loading. The enhancement here reported consists in a considerable breakthrough as far as the lowering of charge recombination phenomena *p*-DSCs is concerned. On the other hand, the optimization of the other cell elements, e.g. dye, electrolyte etc., will be mandatory to further improve the conversion performance of this type of devices in perspective of assembling tandem devices with nanocomposite photocathodes.

## ACKNOWLEDGMENTS

The authors acknowledge the financial support from MIUR which funded the research project PRIN 2010–2011 (protocol no. 20104XET32). DD acknowledges the financial support from the University of Rome “LA SAPIENZA” through the program Ateneo 2012 (Protocol No. C26A124AXX). A.D.C. thanks Regione Lazio and CHOSE for the technical support of the research conducted at the University of Rome “Tor Vergata”. ADC gratefully acknowledges the financial support of the Ministry of Education and Science of The Russian Federation in the framework of Increase Competitiveness Program of NUST «MISiS» (No K2-2017- 025), implemented by a governmental decree dated 16th of March 2013, N 211. Moreover, the authors thank the Center for Nanotechnology Applied to Engineering (CNIS) of the University of Rome LA SAPIENZA for supporting the research and providing access to the DaVinci D8 diffractometer. Authors gratefully acknowledge Prof. Ruggero Caminiti (Director of CNIS Research Centre) for profitable discussion.

## REFERENCES

(1) Yang, W. S.; Park, B. W.; Jung, E. H.; Jeon, N. J.; Kim, Y. C.; Lee, D. U.; Shin, S. S.; Seo, J.; Kim, E. K.; Noh, J. H.; et al. Iodide Management in Formamidinium-Lead-Halide-Based Perovskite Layers for Efficient Solar Cells. *Science (80-. ).* **2017**, *356* (6345), 1376–1379.

(2) Hagfeldt, A.; Boschloo, G.; Sun, L.; Kloo, L.; Pettersson, H. Dye-Sensitized Solar Cells. *Chem. Rev.* **2010**, *110* (11), 6595–6663.

(3) Kakiage, K.; Aoyama, Y.; Yano, T.; Oya, K.; Kyomen, T.; Hanaya, M. Fabrication of a High-Performance Dye-Sensitized Solar Cell with 12.8% Conversion Efficiency Using Organic Silyl-Anchor Dyes. *Chem. Commun.* **2015**, *51* (29), 6315–6317.

(4) Freitag, M.; Teuscher, J.; Saygili, Y.; Zhang, X.; Giordano, F.; Liska, P.; Hua, J.; Zakeeruddin, S. M.; Moser, J.-E.; Grätzel, M.; et al. Dye-Sensitized Solar Cells for Efficient Power Generation under Ambient Lighting. *Nat Phot.* **2017**, *11* (6), 372–378.

(5) Shockley, W.; Queisser, H. J. Detailed Balance Limit of Efficiency of P-n Junction Solar Cells. *J. Appl. Phys.* **1961**, *32*, 510–519.

(6) Perera, I. R.; Daeneke, T.; Makuta, S.; Yu, Z.; Tachibana, Y.; Mishra, A.; Bäuerle, P.; Ohlin, C. A.; Bach, U.; Spiccia, L. Application of the Tris(Acetylacetonato)Iron(III)/(II) Redox Couple in p-Type Dye-Sensitized Solar Cells. *Angew. Chemie - Int. Ed.* **2015**, *54* (12), 3758–3762.

(7) Awais, M.; Gibson, E.; Vos, J. G.; Dowling, D. P.; Hagfeldt, A.; Dini, D. Fabrication of Efficient NiO Photocathodes Prepared via RDS with Novel Routes of Substrate Processing for P-Type Dye-Sensitized Solar Cells. *ChemElectroChem* **2014**, *1*, 384–391.

(8) Sheehan, S.; Naponiello, G.; Odobel, F.; Dowling, D. P.; Di Carlo, A.; Dini, D. Comparison of the Photoelectrochemical Properties of RDS NiO Thin Films for P-Type DSCs with Different Organic and Organometallic Dye-Sensitizers and Evidence of a Direct Correlation between Cell Efficiency and Charge Recombination. *J. Solid State Electrochem.* **2015**, *19* (4), 975–986.

(9) Wei, L.; Jiang, L.; Yuan, S.; Ren, X.; Zhao, Y.; Wang, Z.; Zhang, M.; Shi, L.; Li, D. Valence Band Edge Shifts and Charge-Transfer Dynamics in Li-Doped NiO Based p-Type DSSCs. *Electrochim. Acta* **2016**, *188*, 309.

(10) Borgström, M.; Blart, E.; Boschloo, G.; Mukhtar, E.; Hagfeldt, A.; Hammarström, L.; Odobel, F. Sensitized Hole Injection of Phosphorus Porphyrin into NiO: Toward New Photovoltaic Devices. *J. Phys. Chem. B* **2005**, *109* (48), 22928–22934.

(11) Boschloo, G.; Hagfeldt, A. Characteristics of the Iodide/Triiodide Redox Mediator in Dye-Sensitized Solar Cells. *Acc. Chem. Res.* **2009**, *42* (11), 1819–1826.

(12) Bonomo, M.; Dini, D.; Marrani, A. G. Adsorption Behavior of I3- and I- Ions at a Nanoporous NiO/Acetonitrile Interface Studied by X-Ray Photoelectron Spectroscopy. *Langmuir* **2016**, *32* (44), 11540–11550.

(13) Gibson, E. A.; Le Pleux, L.; Fortage, J.; Pellegrin, Y.; Blart, E.; Odobel, F.; Hagfeldt, A.; Boschloo, G. Role of the Triiodide/Iodide Redox Couple in Dye Regeneration in p-Type Dye-Sensitized Solar Cells. *Langmuir* **2012**, *28* (15), 6485–6493.

(14) Bonomo, M.; Saccone, D.; Magistris, C.; Di Carlo, A.; Barolo, C.; Dini, D. Effect of Alkyl Chain Length on the Sensitizing Action of Substituted Non Symmetric Squaraines for P-Type Dye-Sensitized Solar Cells. *ChemElectroChem* **2017**, *4* (9), 2385–2397.

(15) Bonomo, M.; Carella, A.; Centore, R.; Di Carlo, A.; Dini, D. First Examples of Pyran Based Colorants as Sensitizing Agents of P-Type Dye-Sensitized Solar Cells. *J. Electrochem. Soc.* **2017**, *164* (13).

(16) Ho, P.; Bao, L. Q.; Ahn, K. S.; Cheruku, R.; Kim, J. H. P-Type Dye-Sensitized Solar Cells: Enhanced Performance with a NiO Compact Blocking Layer. *Synth. Met.* **2016**, *217*, 314–321.

(17) Ho, P.; Thogiti, S.; Bao, L. Q.; Cheruku, R.; Ahn, K. S.; Hong Kim, J. Enhanced Efficiency via Blocking Layers at Photocathode Interfaces in Cobalt-Mediated Tandem Dye-Sensitized Solar Cells. *Sol. Energy* **2018**, *161*, 9–16.

(18) Cameron, P. J.; Peter, L. M. How Does Back-Reaction at the Conducting Glass Substrate Influence the Dynamic Photovoltage Response of Nanocrystalline Dye-Sensitized Solar Cells? *J. Phys. Chem. B* **2005**.

(19) Natu, G.; Hasin, P.; Huang, Z.; Ji, Z.; He, M.; Wu, Y. Valence Band-Edge Engineering of Nickel Oxide Nanoparticles via Cobalt Doping for Application in p-Type Dye-Sensitized Solar Cells. *ACS Appl. Mater. Interfaces* **2012**, *4* (11), 5922–5929.

(20) D'Amario, L.; Boschloo, G.; Hagfeldt, A.; Hammarström, L. Tuning of Conductivity and Density of States of NiO Mesoporous Films Used in P-Type DSSCs. *J. Phys. Chem. C* **2014**, *118* (34), 19556–19564.

(21) Itapu, S.; Khan, K.; Georgiev, D. G. Effect of UV Laser Irradiation on the Properties of NiO Films and ZnO/NiO Heterostructures. In *MRS Advances*; 2016; Vol. 1, pp 293–298.

(22) Bonomo, M.; Magistris, C.; Buscaino, R.; Fin, A.; Barolo, C.; Dini, D. Effect of Sodium Hydroxide Pretreatment of $NiO_x$ Cathodes on the Performance of Squaraine-Sensitized *p* -Type Dye-Sensitized Solar Cells. *ChemistrySelect* **2018**, *3* (4), 1066–1075.

(23) Langmar, O.; Saccone, D.; Amat, A.; Fantacci, S.; Viscardi, G.; Barolo, C.; Costa, R. D.; Guldi, D. M. Designing Squaraines to Control Charge Injection and Recombination Processes in NiO-Based Dye-Sensitized Solar Cells. *ChemSusChem* **2017**, *10* (11), 2385–2393.

(24) Favereau, L.; Pellegrin, Y.; Hirsch, L.; Renaud, A.; Planchat, A.; Blart, E.; Louarn, G.; Cario, L.; Jobic, S.; Boujtita, M.; et al. Engineering Processes at the Interface of P-Semiconductor for Enhancing the Open Circuit Voltage in p-Type Dye-Sensitized Solar Cells. *Adv. Energy Mater.* **2017**, *7* (12), 1601776.

(25) Uehara, S.; Sumikura, S.; Suzuki, E.; Mori, S. Retardation of Electron Injection at NiO/Dye/Electrolyte Interface by Aluminium Alkoxide Treatment. *Energy Environ. Sci.* **2010**, *3* (5), 641.

(26) Natu, G.; Huang, Z.; Ji, Z.; Wu, Y. The Effect of an Atomically Deposited Layer of Alumina on NiO in P-Type Dye-Sensitized Solar Cells. *Langmuir* **2012**, *28* (1), 950–956.

(27) Otroshchenko, T. P.; Turakulova, A. O.; Voblikova, V. A.; Sabitova, L. V.; Kutsev, S. V.; Lunin, V. V. NiO and ZrO2-Based Catalysts in the Reaction of Complete Methane Oxidation. *Russ. J. Phys. Chem. A* **2013**, *87* (11), 1804–1808.

(28) Bonomo, M.; Naponiello, G.; Venditti, I.; Zardetto, V.; Carlo, A. Di; Dini, D.; Di Carlo, A.; Dini, D. Electrochemical and

Photoelectrochemical Properties of Screen-Printed Nickel Oxide Thin Films Obtained from Precursor Pastes with Different Compositions. *J. Electrochem. Soc.* **2017**, *164* (2), H137–H147.

(29) Ito, S.; Chen, P.; Comte, P.; Nazeeruddin, M. K.; Liska, P.; Péchy, P.; Grätzel, M. Fabrication of Screen-Printing Pastes from TiO2 Powders for Dye-Sensitised Solar Cells. *Prog. Photovoltaics Res. Appl.* **2007**, *15*, 603–612.

(30) Qin, P.; Zhu, H.; Edvinsson, T.; Boschloo, G.; Hagfeldt, A.; Sun, L. Design of an Organic Chromophore for P-Type Dye-Sensitized Solar Cells. *J. Am. Chem. Soc.* **2008**, *130*, 8570–8571.

(31) Mariani, P.; Vesce, L.; Di Carlo, A. The Role of Printing Techniques for Large-Area Dye Sensitized Solar Cells. *Semicond. Sci. Technol.* **2015**, *30* (10), 104003.

(32) Novelli, V.; Awais, M.; Dowling, D. P.; Dini, D. Electrochemical Characterization of Rapid Discharge Sintering (RDS) NiO Cathodes for Dye-Sensitized Solar Cells of p-Type. *Am. J. Anal. Chem.* **2015**, *6* (2), 176–187.

(33) Wood, C. J.; Summers, G. H.; Clark, C. A.; Kaeffer, N.; Braeutigam, M.; Carbone, L. R.; D'Amario, L.; Fan, K.; Farré, Y.; Narbey, S.; et al. A Comprehensive Comparison of Dye-Sensitized NiO Photocathodes for Solar Energy Conversion. *Phys. Chem. Chem. Phys.* **2016**, *18*, 10727–10738.

(34) Bonomo, M.; Naponiello, G.; Dini, D. Oxidative Dissolution of NiO in Aqueous Electrolyte: An Impedance Study. *J. Electroanal. Chem.* **2018**, *816*, 205–214.

(35) Kumar, K. D. A.; Valanarasu, S.; Jeyadheepan, K.; Kim, H. S.; Vikraman, D. Evaluation of the Physical, Optical, and Electrical Properties of SnO2: F Thin Films Prepared by Nebulized Spray Pyrolysis for Optoelectronics. *J. Mater. Sci. Mater. Electron.* **2018**, *29* (5), 3648–3656.

(36) Qin, P.; Wiberg, J.; Gibson, E. A.; Linder, M.; Li, L.; Brinck, T.; Hagfeldt, A.; Albinsson, B.; Sun, L. Synthesis and Mechanistic Studies of Organic Chromophores with Different Energy Levels for P-Type Dye-Sensitized Solar Cells. *J. Phys. Chem. C* **2010**, *114* (10), 4738–4748.

(37) Koussi-Daoud, S.; Planchat, A.; Renaud, A.; Pellegrin, Y.; Odobel, F.; Pauporté, T. Solvent-Templated Electrodeposition of Mesoporous Nickel Oxide Layers for Solar Cell Applications. *ChemElectroChem* **2017**, *4* (10), 2618–2625.

(38) Klein, Y. M.; Marinakis, N.; Constable, E. C.; Housecroft, C. E. A Phosphonic Acid Anchoring Analogue of the Sensitizer P1 for P-Type Dye-Sensitized Solar Cells. *Crystals* **2018**, *8* (10), 389.

(39) Fabregat-Santiago, F.; Garcia-Belmonte, G.; Bisquert, J.; Zaban, A.; Salvador, P. Decoupling of Transport, Charge Storage, and Interfacial Charge Transfer in the Nanocrystalline TiO2/Electrolyte System by Impedance Methods. *J. Phys. Chem. B* **2002**.